Subgrid Simulations of Reacting Two-Phase Shear Layers*

S. Menon† and S. Pannala‡
School of Aerospace Engineering
Georgia Institute of Technology
Atlanta, GA 30332-0150

ABSTRACT

A two-phase subgrid combustion model has been developed for large-eddy simulations (LES). This approach includes a more fundamental treatment of the effects of the final stages of droplet vaporization, molecular diffusion, chemical reactions and small scale turbulent mixing than other LES closure techniques. In the present approach, the liquid droplets are tracked using the Lagrangian approach up to a pre-specified cut-off size. The phase change of the droplets both larger and smaller than the cut-off size and the subsequent mixing of the evaporated fuel with the oxidizer are modeled within the subgrid using an Eulerian two-phase model. It is shown here that the present approach gives consistently better results for both infinite and finite-rate kinetics in turbulent mixing layer even when the cut-off is increased. In contrast, conventional LES under similar conditions result in significant error when the cut-off size is increased. Finally, as a prelude to the study reacting sprays in realistic gas turbine combustors, a spatially evolving co-axial spray configuration is simulated using a new parallel LES version of the present model. Results are analyzed and discussed to demonstrate the new capability that has been developed.

1. INTRODUCTION

Increasing combustion efficiency, reducing emissions (both NOx and CO) and achieving stable combustion in the lean limit are some of the desirable features for the next generation gas turbine engines. Current research is attempting to improve the atomization process and to increase the fuel-air mixing downstream of the fuel injector. Since, liquid fuel atomization and the subsequent gaseous fuel-air mixing are both highly unsteady, conventional steady state methods cannot be used to elucidate the finer details. The present approach employs the technique of large-eddy simulations (LES). In LES, the scales larger than the grid are computed using a time- and space-accurate scheme, while the unresolved smaller scales are modeled. Closure of momentum transport can be achieved using a subgrid eddy viscosity model since the small scales primarily provide a dissipative mechanism for the energy transferred from the large scales. However, for combustion to occur, the species must first undergo mixing and come into molecular contact. These processes occur at the small scales which are not resolved in the conventional LES. As a result, conventional subgrid models cannot be used to model these features.

To address these issues, a subgrid combustion model was developed and implemented within the LES formulation (Menon et al., 1993; Menon and Calhoon, 1996; Calhoon and Menon, 1996, 1997). This model separately and simultaneously treats the physical processes of molecular diffusion and small scale turbulent convective stirring. This is in contrast to probability density function closure which phenomenologically treats these two processes by a single model, thereby, removing experimentally observed Schmidt number variations of the flow.

The gas-phase methodology was recently extended to two-phase flows (Menon and Pannala, 1997; Pannala and Menon, 1998) to accurately capture the processes of phase change and fuel-air turbulent mixing. In the present paper, this approach has been further refined and used to study both infinite and finite-rate kinetics in a temporally evolving 3D mixing layers. In addition, the implementation of this LES model to simulate spatially evolving 3D sprays is also discussed in this paper.

---

†. Professor, Senior Member, AIAA
‡. GRA, Student Member, AIAA

2. FORMULATION

In the present LES formulation, the two-phase approach is implemented within an Eulerian-Lagrangian approach. Thus, droplets larger than the cut-off size are tracked as in the usual Lagrangian approach and therefore, heat and mass transfer are explicitly computed for each droplet (or group). However, once the droplets are smaller than the cut-off, a two-phase subgrid Eulerian model is employed to include the effects of the small droplets within the LES cells.

Due to resource constraints (computer time and memory), only a limited range of droplet sizes are tracked in a typical Lagrangian simulation. Droplets below an *ad hoc* pre-specified cut-off size are assumed to vaporize instantaneously and to become fully mixed in the gas phase. This is a flawed assumption, since even in gas flows small-scale mixing process is very important for quantitative predictions (Menon and Calhoon, 1996). Recently (Pannala and Menon, 1998), the gas-phase subgrid combustion methodology was extended to account for the final stages of droplet evaporation and turbulent mixing.

Earlier, this approach was demonstrated using the zero-Mach number LES equations (Menon and Pannala, 1997; Pannala and Menon, 1998) for application to low-speed (i.e., incompressible) flows. In the present study, the LES methodology has been extended to compressible flows for the eventual application to combustion problems in realistic gas turbine combustors where acoustic wave motion strongly interacts with the shear flow and the unsteady combustion process.

2.1 Gas Phase LES Equations

The compressible LES equations are obtained by Favre-filtering the Navier-Stokes equations. Here, a top-hat filter (appropriate for finite-volume schemes) is employed. The filtering process results in terms in the resolved LES equations that require modeling. In the following, tilde indicates the LES resolved quantity. The final form of two-phase LES equations for mass, momentum, energy and species.

$$\frac{\partial \bar{\rho}}{\partial t} + \frac{\partial \bar{\rho}\tilde{u}_i}{\partial x_i} = \dot{\rho}_s \tag{1}$$

$$\frac{\partial \bar{\rho}\tilde{u}_i}{\partial t} + \frac{\partial [\bar{\rho}\tilde{u}_i\tilde{u}_j + \bar{p}\delta_{ij} - \bar{\tau}_{ij} + \bar{\tau}_{ij}^{sgs}]}{\partial x_j} = \dot{F}_{s,i} \tag{2}$$

$$\frac{\partial \bar{\rho}\tilde{E}}{\partial t} + \frac{\partial [(\bar{\rho}\tilde{E} + \bar{p})\tilde{u}_i + \bar{q}_i - \tilde{u}_j\bar{\tau}_{ji} + H_i^{sgs} + \sigma_{ij}^{sgs}]}{\partial x_i} = \dot{Q}_s \tag{3}$$

$$\frac{\partial \bar{\rho}\tilde{Y}_\alpha}{\partial t} + \frac{\partial \left[\bar{\rho}\tilde{Y}_\alpha\tilde{u}_i - \bar{\rho}\bar{D}_\alpha\frac{\partial \tilde{Y}_\alpha}{\partial x} + Y_{i,\alpha}^{sgs}\right]}{\partial x_i} = \overline{\dot{\omega}_\alpha} + S_{s,\alpha} \qquad \alpha = 1, N-1 \tag{4}$$

where,

$$\bar{q}_i = -\bar{k}\frac{\partial}{\partial x_i}\tilde{T} + \bar{\rho}\sum_{\alpha=1}^{N}\bar{h}_\alpha\bar{D}_\alpha\frac{\partial \tilde{Y}_\alpha}{\partial x_i} + q_i^{sgs} \tag{5}$$

and $\bar{\tau}_{ij}$ is the resolved viscous stress tensor obtained in terms of the filtered velocity. The above equations would be solved in a conventional LES approach (as noted later, the present approach has a different approach for the solution of the scalar field, Eq. 4). In Eq. (4), $\overline{\dot{\omega}_\alpha}$ is the LES filtered species production/destruction term and N indicates the total number of species.

In the above equations, the source terms $\dot{\rho}_s$, $\dot{F}_s$, $\dot{Q}_s$, and S_s represent, respectively, the volume-averaged rate of exchange of mass, momentum, energy and species between the gas and the liquid phase. These terms are computed, as detailed elsewhere (Oefelein and Yang, 1996; Faeth, 1983).

The above system of equations is supplemented by the equation of state

$$\bar{p} = \bar{\rho}R_u\sum_{\alpha=1}^{N}\{\tilde{Y}_\alpha\tilde{T}/W_\alpha + [\tilde{Y_\alpha T} - \tilde{Y}_\alpha\tilde{T}]/W_\alpha\} \tag{6}$$

where, R_u and W_α are respectively, the universal gas constant and the species molecular weight. Finally, the filtered total energy per unit volume is given by,

$$\bar{\rho}\tilde{E} = \bar{\rho}\tilde{e} + \frac{1}{2}\bar{\rho}\tilde{u}_l\tilde{u}_l + k^{sgs} \tag{7}$$

where,

$$k^{sgs} = \frac{1}{2}\bar{\rho}[\widetilde{u_l u_l} - \tilde{u}_l\tilde{u}_l] \tag{8}$$

is the subgrid kinetic energy which is modeled in the present approach using a transport model (see discussion below). Finally, the filtered internal energy is given by

$$\tilde{e} = \sum_{\alpha=1}^{N} \{\tilde{Y}_\alpha \tilde{h}_\alpha + [\widetilde{Y_\alpha h_\alpha} - \tilde{Y}_\alpha \tilde{h}_\alpha] - \bar{p}/\bar{\rho}\} \qquad (9)$$

which reduces to,

$$\tilde{e} = \sum_{\alpha=1}^{N} \{c_{v,\alpha}\tilde{Y}_\alpha \tilde{T} + c_{v,\alpha}[\widetilde{Y_\alpha T} - \tilde{Y}_\alpha \tilde{T}] + \tilde{Y}_\alpha \Delta h'_{f,\alpha}\} \qquad (10)$$

for calorically perfect gases, where $\Delta h'_{f,\alpha} = \Delta h^0_{f,\alpha} - c_{p,\alpha}T^0$. For thermally perfect gases, the specific heats are usually approximated by polynomials. The higher order subgrid correlations that arise in this case are neglected in this study.

In general, the subgrid terms representing the subgrid stress tensor, the subgrid heat flux, the subgrid viscous work, the subgrid species mass flux, and the subgrid enthalpy flux all require modeling. The exact expressions for these terms are as follows:

$$\begin{cases} \tau_{ij}^{sgs} = \bar{\rho}[\widetilde{u_i u_j} - \tilde{u}_i \tilde{u}_j] \\ H_i^{sgs} = \bar{\rho}[\widetilde{E u_i} - \tilde{E}\tilde{u}_i] + \\ \sigma_{ij}^{sgs} = [\overline{u_j \tau_{ji}} - \tilde{u}_j \tilde{\tau}_{ji}] \\ Y_{i,\alpha}^{sgs} = \bar{\rho}[\widetilde{u_i Y_\alpha} - \tilde{u}_i \tilde{Y}_\alpha] \\ q_i^{sgs} = \bar{\rho}\left[\widetilde{h_\alpha D_\alpha \frac{\partial Y_\alpha}{\partial x_i}} - \tilde{h}_\alpha \bar{D}_\alpha \frac{\partial \tilde{Y}_\alpha}{\partial x_i}\right] \end{cases} \qquad (11)$$

In a conventional LES approach, the subgrid terms τ_{ij}^{sgs}, H_i^{sgs} and $Y_{i,\alpha}^{sgs}$ are modeled while the other terms are neglected. The resulting closure models are:

$$\begin{cases} \tau_{ij}^{sgs} = -2\bar{\rho}\nu_t\left(\tilde{S}_{ij} - \frac{1}{3}\tilde{S}_{ll}\delta_{ij}\right) + \frac{2}{3}\bar{\rho}k^{sgs}\delta_{ij} \\ H_i^{sgs} = -\bar{\rho}\frac{\nu_t}{Pr_t}\frac{\partial}{\partial x_i}\tilde{H} \\ Y_{i,\alpha}^{sgs} = -\bar{\rho}\frac{\nu_t}{Sc_t}\frac{\partial \tilde{Y}_\alpha}{\partial x_i} \end{cases} \qquad (12)$$

where ν_t is the eddy viscosity and $\tilde{S}_{ij}$ is the resolved rate-of-strain tensor. The subgrid eddy viscosity is obtained in terms of the grid scale Δ and the subgrid kinetic energy, k^{sgs} as: $\nu_t = C_\nu \sqrt{k^{sgs}}\Delta$. Here, k^{sgs} is obtained by solving a transport equation (e.g., Menon and Kim, 1996). The coefficient C_ν in the eddy viscosity model and the coefficients appearing in the k^{sgs} equation can be obtained using the dynamic procedure as described elsewhere (Kim and Menon, 1995; Menon and Kim, 1996).

2.2 Liquid-phase LES equations

A Stochastic Separated Flow (SSF) formulation (Faeth, 1983; Oefelein and Yang, 1996) is used to track the droplets using Lagrangian equations of motion. The general equations for spherical droplets reduce to the following form (although, effects of static pressure gradient, virtual-mass, Basset force and external body-forces are neglected here, the inclusion of these terms is not expected to change the current approach):

$$\frac{dx_{p,i}}{dt} = u_{p,i} \qquad (13)$$

$$\frac{du_{p,i}}{dt} = \frac{3}{4}C_D Re_p \frac{\mu}{\rho_p d_p^2}(u_i - u_{p,i}) \qquad (14)$$

where the droplet properties are denoted by subscript p, d_p is the droplet diameter and u_i is the instantaneous gas phase velocities computed at the droplet location. This gas phase velocity field is obtained using both the filtered LES velocity field $\tilde{u}_i$ and the subgrid kinetic energy k^{sgs}. This approach includes stochastic turbulent dispersion effect into the formulation (via the subgrid kinetic energy). As noted earlier, this is not possible using the standard algebraic eddy viscosity subgrid closure. Here, the droplet Reynolds number is: $Re_p = \frac{d_p}{\nu}[(u_i - u_{p,i})(u_i - u_{p,i})]^{1/2}$ and the drag coefficient is (Faeth, 1983):

$$C_D = \begin{cases} \frac{24}{Re_p}\left(1 + \frac{1}{6}Re_p\right) & Re_p \le 10^3 \\ 0.424 & Re_p > 10^3 \end{cases} \qquad (15)$$

The droplet mass conservation is given by: $dm_p/dt = -\dot{m}_p$ where the mass transfer rate for a

droplet in a convective flow field is given as:

$$\frac{\dot{m}_p}{\dot{m}_{Re_p=0}} = 1 + \frac{0.278 Re_p^{1/2} Sc^{1/3}}{[1 + 1.232/Re_p Sc^{2/3}]^{1/2}} \qquad (16)$$

Here, Sc is the Schmidt number and the subscript $Re_p = 0$ indicates quiescent conditions where no velocity difference exists between the gas and the liquid phases. The mass transfer under this condition is $\dot{m}_{Re_p=0} = 2\pi\rho_s D_{sm} d_p ln(1 + B_M)$ and, ρ_s and D_{sm} are, respectively, the gas mixture density and the mixture diffusion coefficient at the droplet surface. Also, B_M is the Spalding number which is given as $B_M = (Y_{s,F} - \tilde{Y}_{\infty,F})/(1 - Y_{s,F})$. Here, $Y_{s,F}$ is the fuel mass fraction at the droplet surface computed as described in Chen and Shuen (1993), while $\tilde{Y}_{\infty,F}$ is the fuel mass fraction in the ambient gas.

The heat transfer rate of the droplet (assuming uniform temperature in the droplet) is (Faeth, 1983):

$$m_p C_{p,p} \frac{dT_p}{dt} = h_p \pi d_p^2 (\tilde{T} - T_p) - \dot{m}_p \Delta h_v \qquad (17)$$

and the heat transfer coefficient for a droplet in a convective flow field with mass transfer is modeled as

$$\frac{h_p}{h_{Re_p=0}} = 1 + \frac{0.278 Re_p^{1/2} Pr^{1/3}}{[1 + 1.232/Re_p Pr^{2/3}]^{1/2}} \qquad (18)$$

Here, Pr is the gas phase Prandtl number and the heat transfer coefficient for quiescent medium is given as $h_{Re_p=0} = \lambda Nu_{Re_p=0}/d_p$ where the Nusselt number is obtained from the relation:

$$Nu_{Re_p=0} = \frac{2 ln(1 + B_M)^{Le^{-1}}}{(1 + B_M)^{Le^{-1}} - 1} \qquad (19)$$

Thus, droplets above the pre-specified cut-off size are solved using the Lagrangian approach and their properties are determined using the above equations. However, a key difference between the conventional droplet tracking method and the present method is that in the new method when the droplets vaporize their phase change effects are incorporated within the subgrid model (described in the next section) whereas in the conventional case these effects are included in the LES resolved species equation (Eq. 4). Only the force term $\dot{F}_{s,i}$ is directly provided to the LES-resolved momentum equations (Eq. 2) in the new approach.

The droplets below the cut-off size are modeled using an Eulerian formulation within the subgrid as described in the next section. In conventional approach, this feature is completely absent and all droplets below the cut-off size are assumed to instantaneously vaporize and mix. This assumption can result in significant error unless the cut-off size is very small. However, reducing the cut-off size to very small number is not always practical since the computational cost rapidly escalates with reduction in drop size. The new formulation of two-phase processes within the subgrid not only improves the accuracy of the scheme, it also allows one to increase the cut-off size without adversely affecting the results. This latter feature is particularly useful since it can drastically reduce the computational effort required for tracking a large group of particles using the Lagrangian method.

In summary, the present LES approach solves only the momentum and energy gas-phase equations on the LES grid. Closure for the subgrid terms in these equations is achieved by using a localized dynamic model for the subgrid kinetic energy (described below). Concurrently, the liquid phase droplet equations for a range of droplet groups are solved using the Lagrangian technique. Stochastic turbulent dispersion of the droplets is included in the present approach using the subgrid turbulent kinetic energy. This capability is not directly available in closures based on the algebraic eddy viscosity model. The phase change, the subsequent fuel-air mixing and the scalar reaction-diffusion processes are modeled within the subgrid as described in the next section.

3. SUBGRID MODELS

Closure of the above LES equations (both gas and liquid phases) requires models for the effect of the subgrid terms on the resolved motion. Two types of closure are needed: a closure for momentum transport and a closure for the scalar transport (both gas and liquid phases). The closure for the momentum transport is achieved by using an eddy viscosity model which is considered reasonable since the small scales are assumed to provide dissipation for the energy transferred from the large scales. The specification of the eddy viscosity requires a length and a velocity (or a time) scale. Many past LES studies have employed an algebraic eddy viscosity model which uses the grid size as the length scale and the resolved rate-of-strain tensor as the time scale (e.g., Germano et al., 1991). However,

this model has some serious limitations. For example, this approach requires equilibrium between turbulent kinetic energy production and dissipation in the small scales which is possible only if a very high resolution LES grid is employed such that only the dissipation scales are unresolved. Such high resolution simulations are not feasible in practice due to resource constraints. By solving for the subgrid kinetic energy (which also gives an appropriate velocity scale for subgrid closure), the equilibrium requirement can be relaxed and coarser grid LES is possible. Furthermore, to model turbulent dispersion of particles the subgrid kinetic energy provides the required information which is absent in the algebraic model closure.

3.1 The Subgrid Momentum Closure

The subgrid closure of the unresolved stresses and energy flux is achieved in the present approach by solving a transport model for the subgrid kinetic energy, k^{sgs}. Details have been reported elsewhere. Here, the extension of the earlier model for gas phase to two-phase flows has been carried out. The final form is:

$$\frac{\partial \bar{\rho} k^{sgs}}{\partial t} + \frac{\partial}{\partial x_i}(\bar{\rho}\tilde{u}_i k^{sgs}) = T_k + P_k - D_k + F_k \qquad (20)$$

Here, $T_k = \frac{\partial}{\partial x_i}\left(\frac{\nu_t}{\sigma_k}\frac{\partial k^{sgs}}{\partial x_i}\right)$ is the transport term and $\sigma_k \approx 1.$ is a constant. The other terms, P_k and D_k are respectively, production and dissipation of k^{sgs}. The last term F_k is unique to two-phase flows and represents the work done due to the two-phase coupling force term $\dot{F}_{s,i}$. This term (similar to terms in the LES equations, Eq. 2) provides the coupling between the turbulent motion of the droplets and the evolution of the subgrid kinetic energy. The closure of Eq. (20) is obtained using $P_k = -\tau_{ij}^{sgs}\tilde{S}_{ij}$, $D_k = C_\varepsilon \bar{\rho}\frac{k^{sgs3/2}}{\Delta}$ and

$$F_k = \tilde{\dot{F}}_{s,i}\tilde{u}_i - \tilde{\dot{F}}_{s,i}\tilde{u}_i \qquad (21)$$

Here, C_ε is another coefficient that must be obtained (along with C_ν) using the dynamic procedure.

The expression in Eq. (21) represents the direct effect of two-phase coupling on k^{sgs} and requires modeling. Note that, k^{sgs} is indirectly modified due to particle motion and vaporization since the force term $\dot{F}_{s,i}$ will change the resolved velocity field (via Eq. 2) which in turn will change the resolved subgrid kinetic energy. Inclusion of the term F_k allows for an additional (direct) modification of the subgrid kinetic energy due to interaction between the particles and the *unresolved* small scale motion. At present, it is not clear how to model this term and therefore, this term is currently neglected. An effort is planned using direct simulations to study particle motion and vaporization in a fully resolved turbulent homogeneous field (similar to studies reported earlier, Squires and Eaton, 1989 and Elgobashi and Truesdell, 1992). This study should provide information on how the kinetic energy spectrum at the small scales (albeit in a relatively low Reynolds number flow) is modified due to droplets.

Thus, the presence of the droplets can have a two-fold effect. The first effect is directly on the LES resolved momentum transport due to the coupling force term, $\dot{F}_{s,i}$. The second effect is the modification to the subgrid kinetic energy due to the force term Eq. 21 which accounts for the interaction between the particles and the small-scale unresolved turbulent field.

3.2 The Subgrid Species Closure

The principle difficulty in reacting LES simulations is the proper modeling of the combustion related terms involving temperature and species, for example, the convective species fluxes such as $Y_{i,\alpha}^{sgs}$ due to subgrid fluctuations and the filtered species mass production rate $\overline{\dot{\omega}_\alpha}$. Probability density function methods when applied within LES either using assumed shape or evolution equation may be used to close $\overline{\dot{\omega}_\alpha}$ and, in principle, any scalar correlations. However, the treatment of molecular mixing and small scale stirring using phenomenological models as in pdf methods, have not been very successful in predicting the mixing effects. Problems have also been noted when the gradient diffusion model is used to approximate the species transport terms.

The linear eddy mixing (LEM) model (Kerstein, 1989) treats separately molecular diffusion and turbulent mixing processes at all relevant length scales of the flow. The scalar fields are simulated within a 1D domain which, in the context of LES, represents a 1D slice of the subgrid flame brush. The subgrid model simulates only the effect of the small unresolved scales on the scalar fields while the larger resolved turbulent scales of the flow are simulated by the LES equations. The subgrid LEM has several advantages over conventional LES of reacting flows. In addition to

providing an accurate treatment of the small-scale turbulent mixing and molecular diffusion processes, this method avoids gradient diffusion modeling of scalar transport. Thus, both co- and counter-gradient diffusion can be simulated. More details of this approach (which is identical to the method used for gas phase LES) is given elsewhere (Menon and Calhoon, 1996; Calhoon and Menon, 1996, 1997) and therefore, avoided here.

3.2.1 The Single Phase Model

In the baseline model the exact reaction-diffusion equations are numerically solved using a finite-difference scheme in the local subgrid 1D domain using a grid fine enough to resolve the Kolmogorov and/or the Batchelor microscales. Consequently, the production rate $\dot{\omega}_\alpha$ can be specified in the subgrid without any modeling. Simultaneous to the deterministic evolution of the reaction-diffusion processes, turbulent convective stirring within the 1D domain is modeled by a stochastic mapping process (Kerstein, 1992). This procedure models the effect of turbulent eddies on the scalar fields and is implemented as an instantaneous rearrangement of the scalar fields without changing the magnitudes of the individual fluid elements, consistent with the concept of turbulent stirring.

The implementation of the stirring process requires (randomly) determining the eddy size l from a length scale pdf $f(l)$ in the range $\eta \le l \le l_{LEM}$ where η is the Kolmogorov scale and l_{LEM} is the characteristic subgrid length scale which is currently assumed to be the local grid resolution Δ. A key feature of this approach is that this range of scales is determined from inertial range scaling as in 3D turbulence for a given subgrid Reynolds number: $Re_{LEM} = u' l_{LEM}/\nu$ where, u' is obtained from k^{sgs}. Thus, the range of eddy sizes and the stirring frequency (or event time) incorporates the fact that the small scales are 3D. This feature is one of the major reasons for the past successes of LEM in gas phase diffusion flame studies (Menon and Calhoon, 1996; Calhoon and Menon, 1996, 1997).

A new feature for two-phase flows needs to be considered in this formulation. For example, the above noted stirring process uses inertial range scaling laws which do not account for the presence of droplets. If, however, droplet motion and vaporization changes the turbulent spectra in the inertial range from the well known -5/3 law of Kolmogorov, then this information needs to be incorporated. The above noted DNS study will be used to determine the changes if any to the turbulence spectra. Modifications to $f(l)$ and the event frequency (both of which uses inertial range scaling rules) can then be made to account for effect of droplets on the turbulent field. Results using these changes will be reported in the near future.

3.2.2 The Two-Phase Model

For two-phase flows, the LEM reaction-diffusion equations have been modified to include two new features: (a) the vaporization of the droplets tracked by the Lagrangian method, and (b) the vaporization of droplets below the cut-off so that the final stages of droplet vaporization and mixing is included. However, some changes are required since droplet vaporization will change the subgrid mass of the gas (primarily the fuel). Thus, in addition to the scalar reaction-diffusion equations, the two-phase mass conservation equations must be solved in the subgrid.

The droplets below the cutoff have been included by assuming that the droplets act as a psuedo-fluid and therefore, the overall effect of the droplets within each LES cell can be modeled as a void fraction. This approach is valid only when the droplets form only a small fraction of the total volume. However, this is an acceptable assumption here since all droplets larger than the cut-off are still tracked using the Lagrangian approach. The present Eulerian two-phase approach is also preferred (in terms of accuracy) when compared to the Lagrangian approach when the droplets are very small and begin to behave more like a continuum fluid.

Mass conservation in both the phases in the LEM is given by: $\rho_g \varphi + \rho_l (1-\varphi) = \rho_{avg}$, where subscript g represents gas phase, l the liquid phase and φ is the volume fraction of the gas phase (1 - void fraction of the liquid (λ)). The void fraction λ or φ evolve during the subgrid evolution. Although, the liquid density is a constant, the gas density ρ_g changes and needs to be determined. The mass conservation of each phase is imposed in the subgrid scales and are obtained from the following equations:

$$\frac{\partial \rho_g \varphi}{\partial t} = S_L + S_2 \qquad (22)$$

and

$$\frac{\partial (1-\varphi)\rho_l}{\partial t} = S_1 - S_2 \qquad (23)$$

Here, the source term S_1 is the contribution of the supergrid droplets (i.e., the LES-resolved Lagrangian droplets) to the subgrid liquid phase when the droplet size falls below the cutoff. S_L is due to vaporization of the droplets tracked in the supergrid and S_2 represents vaporization of liquid in the subgrid.

The gas phase species equation for any scalar mass fraction (Ψ) in the subgrid can be written as

$$\frac{\partial \rho_g \varphi\psi}{\partial t} = D\frac{\partial^2(\rho_g \varphi\psi)}{\partial s^2} + \dot{\omega}_\psi + S_\psi + S_L \qquad (24)$$

Here, "s" indicates the 1D domain of LEM. Also, S_ψ is the source term (only in the fuel species equation) for production due to vaporization of the liquid phase. An equation for temperature must also be solved with the above equations since vaporization requires heat absorption and is followed by a drop in temperature. This is quite similar to the method used in the earlier gas phase studies of heat release effect (Calhoon and Menon, 1997).

Note that, in Eqs. (22-24) the convective terms are missing. This is consistent with the LEM approach, whereby, the convection of the scalar fields is modeled using two distinct and concurrent processes: the small-scale turbulent stirring which accounts for convection in the small scales and the splicing process which accounts for convection of scalars at the LES resolved scales. Some comments regarding the large-scale convection process is given in the next section.

3.3 Subgrid implementation

Since the filtered species $\tilde{Y}_\alpha$ and the mixture density $\bar{\rho}$ are calculated directly by filtering the subgrid Y_α and ρ_{avg} fields, there is no need to solve the equivalent LES filtered mixture mass and species conservation equations (i.e., Eqs. 1 and 4). Consequently, use of conventional (gradient diffusion) models is avoided. However, since both Y_α and ρ_{avg} subgrid fields are also influenced by large scale convection (due to the velocity field $\tilde{u}_i$ and the subgrid turbulent fluctuation estimated from k^{sgs}), additional coupling processes are required.

The convection of the scalar fields by the LES field across LES cell faces is modeled by a "splicing" algorithm (Menon et al., 1993; Menon and Calhoon, 1996; Calhoon and Menon, 1996). Details of this process are given in the cited references. Given the initial subgrid scalar fields and void fraction, droplet vaporization, reaction-diffusion, turbulent stirring, and large scale convection processes are implemented as discrete events within each LES cell. The epochs of these processes are determined by their respective time scales.

The splicing algorithm transports subgrid fluid elements from one LES cell to another based on the local velocity field. The local velocity consists of the resolved velocity $\tilde{u}_i$ plus a fluctuating component (estimated from the subgrid kinetic energy). The splicing events are implemented discretely on the convective time scale. Each splicing event involves (1) the determination of volume transfer between adjacent LES grid cells, (2) the identification of the subgrid elements to be transferred, and (3) the actual transport of the identified fluid elements. The underlying rationale for this procedure has been discussed elsewhere (Menon et al., 1993; Calhoon and Menon, 1996). The same algorithm is used here.

An important property of the splicing algorithm is that the species convection is treated as in Lagrangian schemes. Thus, convection is independent of the magnitude or gradient of the species which are transported and depends only on the velocity field. This property allows this algorithm to avoid false diffusion associated with numerical approximation of convective terms in differential equations. By avoiding both numerical and gradient diffusion, the splicing algorithm allows an accurate picture of the small scale effects of molecular diffusion to be captured, including counter-gradient and differential diffusion effects.

In the present two-phase implementation, the subgrid liquid void fraction is also transported across LES cells based on the volume transfer of the gas phase. This process is not strictly correct since the liquid phase transport should be based on the liquid volume transfer across LES cell. A method to deal with this transport has been developed and will be used in future studies.

4. PARALLEL IMPLEMENTATION

The technique of data concurrency (i.e., the primary data space is partitioned and distributed among the processors) rather than functional concurrency (i.e., the overall application is decomposed into several distinct parallel computational tasks) was chosen after careful review of the type and degree of parallelism inherent in the numerical algorithm used for LES. The data space is partitioned and distributed to the processors so that 1) the distribution of cells to the nodes leads to a nearly balanced load of communication and computation among all nodes, and 2) the inherent spatial data locality of the underlying cell structure is

maintained so as to minimize interprocessor communication. The cell-partitioning scheme decomposes the 3D computational domain into logically congruent, nearly equal-sized rectangles (cubes). Maximum concurrency is extracted to minimize the execution time on a given number of processors.

In the present implementation, the partitioning scheme results in each processor performing computations only on the cells held by it. For finite-difference or finite-volume schemes, each domain contains extra layers of ghost cells along the processor partitions to allow the exchange of boundary cell data. This exchange is carried out using a few relatively long messages. As a result, the high cost of latency associated with message passing is minimized, resulting in a reduced communication overhead even though this data exchange results in an increased memory overhead.

The parallel implementation of the Lagrangian droplet tracking model is more problematic mainly because the spatial distribution of the droplets is not uniform and is changing with time. Load balancing can become a serious issue in this case. At present, all the droplets are initialized on a single processor and this information is broadcast to all the processors. At the end of this stage, each processor takes ownership of the droplets only within its domain. Then, all the droplet equations are integrated in parallel on all the processors. At end of each LES cycle, the droplets are again mapped to a single processor to re-assign their locations within the computational domain. Although, this procedure might lead to some load imbalance, by proper mapping of the physical problem onto the processors, this problem can be greatly alleviated. The present procedure has the distinct advantage of keeping the inter-processor communication to a minimum. Further optimization of the parallelization of the liquid phase is planned in the near future.

The implementation of the subgrid combustion model within the LES method is relatively straightforward since the subgrid model resides within the LES cells and requires no inter-cell communication for the local subgrid processes. However, inter-processor communication is needed every LES time step to transport the subgrid scalar field across LES cell surfaces. These messages carry the local scalar information. However, unlike the long messages needed for the fluid dynamics part, these messages are from the nearest neighbor cells and thus, are relatively short messages.

The efficiency of this parallel LES solver (at least the gas phase version) has been discussed extensively in earlier studies and therefore, is not repeated here.

5. RESULTS AND DISCUSSION

The two-phase subgrid model has been implemented into both a zero-Mach Number code and a 3D compressible code. The zero-Mach number code is a finite-difference semi-implicit solver that is second-order accurate in time, and uses a fifth-order upwind biased stencil for the convective terms, a fourth-order central scheme for the viscous terms and a second-order scheme for the solution of the Poisson equation for pressure. The compressible code is a finite volume formulation that is second order accurate in time and fourth-order accurate in space. Details of both these codes have been reported in numerous cited reference and therefore, is avoided here for brevity.

The Lagrangian tracking of the droplets is carried out using a fourth-order Runge-Kutta scheme and the gas phase velocity at the droplet location is obtained using a fourth order interpolation scheme.

In the following, the discussion focuses primarily on ability of the new subgrid two-phase model and on the demonstration of this LES code for simulating spatially evolving sprays. The ability of the new method is reviewed by direct comparison with the conventional LES approach where the species equations are solved along with the other LES equations and a dynamic eddy diffusivity model is employed for closure.

5.1 Droplet Vaporization in a Mixing Layer

For these studies, droplets were injected into the core of a temporal mixing layer at time t=0. The mixing layer is initialized by a tangent hyperbolic mean velocity along with the most unstable 2D (of dimensional wavelength 2π) mode and random 3D turbulence (similar to that described in Metcalfe et al., 1987). Earlier, results (for relatively low Reynolds number) were obtained using grid resolution of 32x32x32 and 64x64x64 and compared. Comparison showed good agreement indicating grid independence.

The mixing layer is initialized with the oxidizer in both the upper and lower streams at 350 K and the fuel droplets are initially introduced in the mid-plane. A range of droplets from 10-50 micron radius with an initial temperature of 300 K was used for all simulations with the droplet cut-off radius at 5 micron. A total of 2100 droplet groups were tracked (the effect of varying the droplet group has not yet been carried out). For simplicity, the droplet groups were uniformly distributed and the number of droplets in each group is chosen such that the overall mass loading is 0.5 which corresponds to a volume loading of 0.0005.

Simulations using the new subgrid model have been compared to conventional simulations. For these

studies, a subgrid resolution that captured the effect of turbulent stirring by the largest small scales (here, for simplicity, a subgrid eddy size 60% of the grid resolution is used), was used to reduce the computational cost. Subgrid resolution was doubled and similar results were obtained indicating that the present tests captures the effect of the largest subgrid scales quite accurately.

Note that if the droplet cutoff size is chosen such that no droplet falls below the cutoff, then the void fraction is zero. In this case, the present LES and the conventional LES approaches should agree reasonably well. The only difference between the two approaches is that the new approach simulates the scalar fields in the subgrid and therefore, the phase change of the Lagrangian droplets will appear as a source term (S_L) in the subgrid gas density and the subgrid fuel species equations (Eqs. 22 and 24). In contrast, the conventional LES will solve the species conservation equations along with the other LES equations and phase change source term will be used in Eq. 4.

Calculations using infinite rate kinetics (when the vaporized fuel mixes with the oxidizer and instantaneously reacts) were carried out for the case when all drops (even when they vaporize) are larger than the cutoff size. The product mass fraction (ratio of the product density to the overall gas density) predicted by the conventional and the new LES approaches are compared in Fig. 1a. It can be seen that there is very good agreement between the two methods thereby confirming the validity of the new LES approach. The predicted temperature of the gas phase (Fig. 1b) also shows good agreement.

The conventional LES assumes that as droplets fall below the cut-off size they instantaneously vaporize and mix. This can result in significant error especially if the cut-off size is large. As a result, to maintain good accuracy, conventional LES requires a very small cut-off size. This, in turn, increases the computational cost considerably. Since the new subgrid approach is supposed to take care of the vaporization process even in the subgrid, it should be able to deal with an increased cut-off size without adversely affecting the accuracy. This has been demonstrated by simulating identical problems but with different cut-off sizes of 10 and 20 microns.

The subgrid void fraction models, Eqs. 22 and 23, have no explicit droplet size information other than in the source terms. The source term S_2 represents the vaporization of the liquid in the subgrid and is (in general) a function of the droplet size. The expression is same as in Eq. 16. It was determined that as the droplet cut-off size is increased, the subgrid vaporization model for S_2 needs to represent the droplet distribution from the cut-off to the smallest possible size. This requirement is qualitatively similar to the need to characterize (and pick) the eddy size that causes the turbulent mixing process in the subgrid (as described in section 3.2.1. To account for this, the S_2 term (Eq. 16) picks a representative droplet size from a distribution within the subgrid. In general, the droplet size should be picked at random from the distribution similar to the manner the eddy size is picked for turbulent stirring. However, at present, the droplet sizes are picked using representative drop sizes. For example, for a cut-off size of 20 micron, the source term S_2 was estimated by choosing a drop size of 20 micron with a probability of 0.67 and by choosing a 15 micron size with a probability of 0.33. This procedure still needs to be investigated and refined further and will be addressed in the near future.

Another issue is the afore mentioned issue regarding the transport of the subgrid liquid void fraction across the LES cells. A method to deal with this transport has been developed and will be used in future studies.

In spite of these concerns, the new approach shows significant advantage over the conventional approach. For example, the product mass fraction obtained by the two LES methods are compared in Figs. 2a and 2b, respectively, for the various cut-off sizes. The results predicted by the conventional LES are in gross error for cut-off radius of 10 and 20 micron. However, the present methodology agrees very well over the cutoff range. Ideally, the subgrid model should predict identical results for a range of cut-off sizes. The observed differences in the spread are due to slightly higher vaporization rates in the peripherals of the mixing layer. This may be related to the afore mentioned issue regarding transport of the liquid void fraction across LES cells. A correction to this approach is being developed and will be used to re-evaluate this effect.

The above results clearly suggest that with the new approach a larger cut-off size can be used without a loss of accuracy. This has important implications for computational effort since the present subgrid approach is much more expensive when compared to the conventional method for the same cut-off size. Thus, increasing the cut-off size should offset the increased cost of the subgrid model. In fact, preliminary estimates suggest that a conventional LES using 15,000 particles and a cut-off size of 2.5 micron is nearly 4-5 times more expensive than the subgrid LES approach which used a 10 micron cut-off. This result provides

confidence that the new approach will be both more cost effective and more accurate than the conventional approach.

Finite-rate (Damkohler number) effects (but with no heat release) were also investigated earlier (Pannala and Menon, 1998). It was shown that as the chemical time scale decreases (Da increases), the product mass fraction increases, in agreement with earlier results and physics. Due to finite-rate effects, there is a considerable amount of unreacted fuel in the gaseous form. In addition to the droplet temperature and the surrounding oxidizer concentration, the amount of fuel present in the gaseous form dictates the liquid to gaseous fuel phase change. Thus, the vaporization rate is coupled to the rate of chemical kinetics, heat release and the other processes such as convection. using the two different approaches and compared.

The new approach is able capture the Da-effects without error when the cut-off size is increased. For example, the product mass fractions for a Da=100 case computed using the conventional approach are shown for various cut-off sizes in Fig. 3a and the corresponding results obtained using the new LES approach are shown in Fig. 3b. As seen earlier for the infinite-rate kinetics, increasing the cut-off does not adversely affect the predictions by the present LES whereas, the conventional LES results in significant errors.

Although it appears that the new method can capture Da-effects this capability needs to be reevaluated in the presence of heat release. Furthermore, since the present method can deal with differential diffusion quite easily, Lewis number effects can also be studied. This will be demonstrated in the near future.

5.2 Droplet Motion in a Spatial Shear Layer

The above study provided confidence that the present approach has some significant advantages over the conventional LES approach. However, to fully demonstrate this method, detailed validation against experimental data is required. Unfortunately, controlled experiments where all the required information is obtained is almost non-existent. To address this issue, an experimental program is underway at Georgia Tech where a co-axial shear layer configuration has been built with a liquid fuel injector in the inner pipe to obtain detailed data for code validation. This configuration is shown schematically in Fig. 4. A key feature of this device is that the liquid fuel in injected inside the inner pipe. Therefore, the liquid jet breakup, the initial droplet formation and the dense spray regime all occur inside the inner pipe. By properly choosing the location of the liquid fuel injector relative to the exit plane, a dilute spray can be made to form and to exit from the inner pipe. In this manner, the inflow spray distribution is dilute and the inflow properties (for both the gas and liquid phases) can be carefully measured using laser Doppler velocimetry and phased Doppler anemometry techniques. This information can then be used to initialize the LES and then the ability of the code to predict the distribution at a downstream location can be used to evaluate the accuracy of the new method.

Currently, the experiments are underway using a water spray to mimic non-evaporating particle motion and data is still being acquired. Subsequently, experiments using an acetone spray is planned to investigate vaporizing droplets. To get ready for this phase of study, the present LES model has been implemented into a 3D parallel, spatial compressible code and preliminary calculations have been performed to evaluate the new code. Some characteristic results are discussed.

Simulations were carried out with the two-phase LES code for the configuration shown in Fig. 4. A resolution of 65x65x33 was used to resolve the axisymmetric 3D domain. The axial extent of the computational domain was 25D where D is the diameter of the inner pipe. Droplets were injected into the domain every 5 LES time step. Thus, the number of droplet groups initially increase till around 10,000 groups are present in the stationary state. The droplet size distribution was varied to evaluate its effect on turbulent dispersion. Two cases are discussed below: a case with a uniform fixed size droplet distribution and a case with a log-normal distribution very similar to the distribution obtained in our experimental facility.

Figure 5a shows the spanwise vorticity contours for the simulated co-axial jet. The spatial droplet distribution for a simulation with a single size particles (radius of 20 micron) and for a simulation with a log normal distribution (similar to the experiments) are shown respectively, in Figs. 5b and 5c (not that axial scale has been compressed for better visualization). Both of these cases are unforced and it can be observed that shear layer goes unstable few diameters downstream of the jet exit. As expected, till that point the lateral dispersion of the particles is insignificant. Further downstream, as the shear layer becomes unstable and starts to rollup, there is an increased dispersion of the droplets in the radial direction. This can be seen in Figs. 5b and 5c. In the log-normal case (Fig. 5c), the range of droplets tracked vary from Stokes Number of 0.01 to 10.0. The smaller droplets (small Stokes Number) follow the gas flow very closely as seen in Fig. 5c while the particles with larger Stokes

No. encounter more drag and have paths that no longer follow the gas motion.

Figure 6a shows the spanwise vorticity contours for the case (using a log-normal droplet distribution) with the inner jet forced at a frequency corresponding to a Strouhal Number of 0.3 based on the inner jet diameter and average velocity in the inner jet. This frequency corresponds to the jet preferred mode of the inner jet and should cause the shear layer to go unstable and roll up into large vortical structures. This can be observed in this figure. The effect of forcing also significantly changes the particle dispersion in the shear layer. This can be seen in Fig. 6b which shows that particle dispersion significantly increased in the forced case. Also observed in this figure is the gaps in the droplet scatter. This is due to the centifuge effect of the particles of Stokes number of order one caused by the formation and motion of large vortical structures. The peak of the log-normal distribution used in the present study is around a droplet size of 60 micron, which is the appropriate size for the centrifuge effect. This effect is very similar to what was observed in the forced shear layer experiments of Lazaro and Lasheras (1992), as well as in the earlier simulations of temporal mixing layers (Martin and Meiburg, 1994; Pannala and Menon, 1998). These results confirm at least qualitatively, that the present spatial implementation of the two-phase LES model is performing as expected.

In order to quantify the above behavior, Sauter mean diameter (D32) is plotted against the radial distance (normalized by the inner jet diameter) in Fig. 7a. Due to increased lateral dispersion of the bigger droplets (Stokes number ~ 1) there is an increase in the SMD in the peripherals of the shear layer. There is also a dip corresponding to the locations of strong vortical structures. The number of droplets (calculated based on SMD) are plotted against the radial distance in Fig. 7b. This plot clearly shows the strong effect of forcing in the lateral dispersion of particles.

In summary, the two-phase LES model has been implemented in a parallel 3D compressible LES code to study realistic spray combustion in gas turbine combustors. At present only qualitative results (which appear physically consistent) have been obtained using this code. Detailed validation for both non-evaporating and evaporating droplets (and using high grid resolution LES) are planned using results from an experimental study that has been particularly designed for code validation. This validation study will be reported in the near future. Subsequently, this LES code will be employed to study reacting cases with heat release with an eventual goal of developing a methodology to study actively controlled spray combustion.

6. CONCLUSIONS

In this study, a subgrid combustion model for two-phase flows has been developed and validated for simple turbulent shear flow cases. The proposed LES approach includes a more fundamental treatment of the effects of the final stages of droplet vaporization, molecular diffusion, chemical reactions and small scale turbulent stirring than other LES closure techniques. As a result, Reynolds, Lewis and Damkohler number effects are explicitly included and can be correctly predicted. A key feature of this Eulerian-Lagrangian two phase formulation is that the vaporization of the Lagrangian droplets and the evaporation and mixing of the droplets smaller than the cut-off size are modeled within the subgrid using an Eulerian two-phase model that is an extension of the earlier gas-phase subgrid model.

The results presented here (and others discussed earlier in Menon and Pannala, 1997; Pannala and Menon, 1998) show that many features observed in experiments have been captured by this method. For example, using a temporally evolving 3D mixing layer, it has been shown earlier that the increased dispersion of non-vaporizing droplets at intermediate sizes in forced mixing layers agrees well with trends seen in earlier experimental and numerical studies. When vaporization was included, modifications to the vortex structure was found to be due to the production of baroclinic torque. This result is quite similar to the heat release effect seen earlier in single phase mixing layers. In the present study, it has been shown that when the droplet cut-off size is increased, the conventional method gives erroneous results while the current methodology provides very accurate predictions for both infinite and finite-rate kinetics. It has also been shown that the present approach could be computationally more efficient (in-spite of the increased cost of the subgrid model) because it can use a larger cut-off size without any loss of accuracy.

Based on these studies, the LES model has been implemented in a parallel, 3D compressible solver to study spatially evolving reacting liquid sprays. To validate this code, a configuration identical to an experimental co-axial two-phase spray geometry is modeled and preliminary results for both unforced and forced cases have been obtained. The configuration and the test conditions have been chosen to match the experimental case. Thus, once the inflow conditions become available from the experiments, detailed LES of this flow problem will be carried out to validate this approach. Results from these studies will be reported in the near future.

ACKNOWLEDGMENTS

This work was supported by the Army Research Office Multidisciplinary University Research Initiative grant DAAH04-96-1-0008. Computations were carried out under the DoD HPC Grand Challenge Project at the Origin 2000 at ARC, Huntsville, AL and the Cray T3E at NAVO, Stennis Space Center, MS.

REFERENCES

Calhoon, W.H. and Menon, S. (1996) "Subgrid Modeling for Reacting Large-Eddy Simulations," AIAA 96-0516, 34th AIAA Aerospace Sciences Meeting.

Calhoon, W.H. and Menon, S. (1997) "Linear-Eddy Subgrid Model for Reacting Large-Eddy Simulations: Heat Release Effects," AIAA 97-0368, 35th AIAA Aerospace Sciences Meeting.

Elgobashi, S. E. and Truesdell, G. C. (1992) "Direct Simulation of Particle Dispersion in a Decaying Isotropic Turbulence," Journal of Fluid Mechanics, Vol. 242, 655-700.

Faeth, G. M. (1983) "Evaporation and Combustion of Sprays," Progress in Energy and Combustion Science, Vol. 9, pp. 1-76.

Kerstein, A. R. (1989) "Linear-Eddy Model of Turbulent Transport II. Application to Shear Layer Mixing," Combustion and Flame, Vol. 75, pp. 397-413.

Kerstein, A. R. (1992) "Linear-Eddy Model of Turbulent Transport 4. Structure of Diffusion-Flames," Comb. Sci. and Tech., Vol. 81, pp.75-96.

Kim, W.-W. and Menon, S. (1995) "A New Dynamic One-equation Subgrid-scale Model to Turbulent Wall-bounded Flows," AIAA 95-0356, 33rd AIAA Aerospace Sciences Meeting.

Lazaro, B. J., and Lasheras, J. C. (1992a) "Particle Dispersion in the Developing Free Shear Layer," J. Fluid Mech., Vol. 235, pp. 143-178.

Lazaro, B. J., and Lasheras, J. C. (1992b) "Particle Dispersion in the Developing Free Shear Layer," J. Fluid Mech., Vol. 235, pp. 179-221.

Martin, J. E. and Meiburg, E. (1994) "The Accumulation and Dispersion of Heavy Particles in Forced Two-dimensional Mixing Layers. I. The Fundamental and Subharmonic Cases," Phys. Fluids, Vol. 6 (3), pp. 1116-1132.

Menon, S., McMurtry, P., and Kerstein, A.R. (1993a) "A Linear Eddy Mixing Model for LES of Turbulent Combustion," in Large-Eddy Simulations of Complex Engineering and Geophysical Flows, (B. Galperin and S.A. Orszag, Eds.), Cambridge Univ. Press, pp. 278-315.

Menon, S. and Kim, W.-W. (1996) "High Reynolds Number Flow Simulations using the Localized Dynamic Subgrid-Scale Model," AIAA 96-0425, 34th AIAA Aerospace Sciences Meeting.

Menon, S. and Calhoon, W. (1996) "Subgrid Mixing and Molecular Transport Modeling for Large-Eddy Simulations of Turbulent Reacting Flows," Symp. (International) on Combustion, 26, 59-66.

Menon, S. and Pannala, S., "Subgrid Modeling of Unsteady Two-Phase Turbulent Flows," AIAA Paper No. 97-3113, 33rd AIAA/ASME/SAE/ASEE Joint Propulsion Conference and Exhibit, Seattle, WA, July 6-9, 1997.

Metcalfe, R. W., Orszag, S. A., Brachet, M. E., Menon, S., and Riley, J. J. (1987) "Secondary Instability of a Temporally Growing Mixing Layer," J. Fluid Mech., Vol. 184, pp. 207-243.

Mostafa, A. A. and Mongia, H. C. (1983) "On the Modeling of Turbulent Evaporating Sprays: Eulerian versus Lagrangian Approach," Int. J. of Heat Mass Transfer, Vol. 30, pp. 2583-2593.

Oefelein, J. C. and Yang, V. (1996) "Analysis of Transcritical Spray Phenomena in Turbulent Mixing Layers," AIAA 96-0085, 34th AIAA Aerospace Sciences Meeting.

Pannala, S. and Menon, S. (1998) "Large Eddy Simulations of Two-Phase Turbulent Flows," AIAA 98-0163, 36th AIAA Aerospace Sciences Meeting.

Squires, K. D., and Eaton, J. K. (1989) "Study of the Effects of Particle Loading on Homogenous Turbulence using Direct Numerical Simulation," Proceedings International Symposium on Turbulence Modification in Dispersed Multiphase Flows, San Diego, CA.

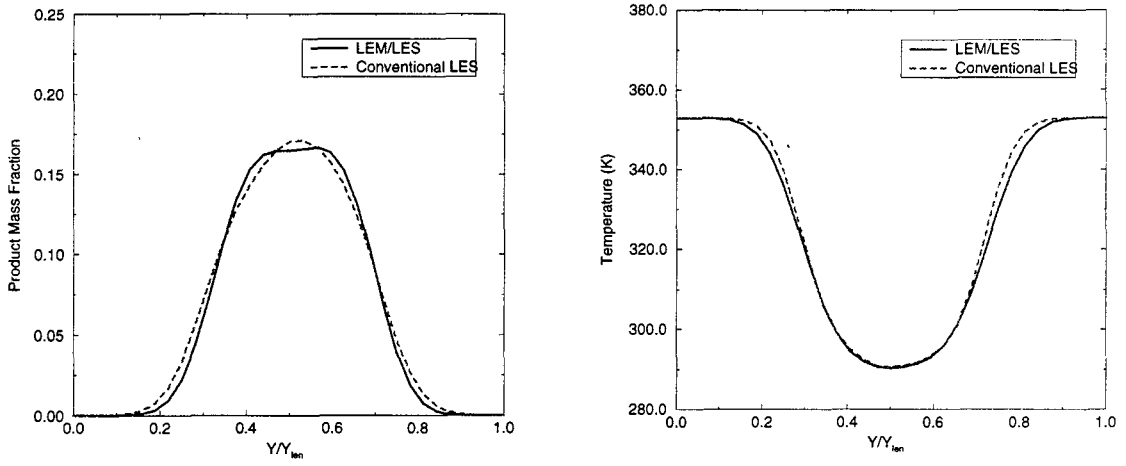

Figure 1: Comparison of conventional and current methodology. (a) Variation of product mass fraction across the mixing layer and (b) Variation of temperature across the mixing layer.

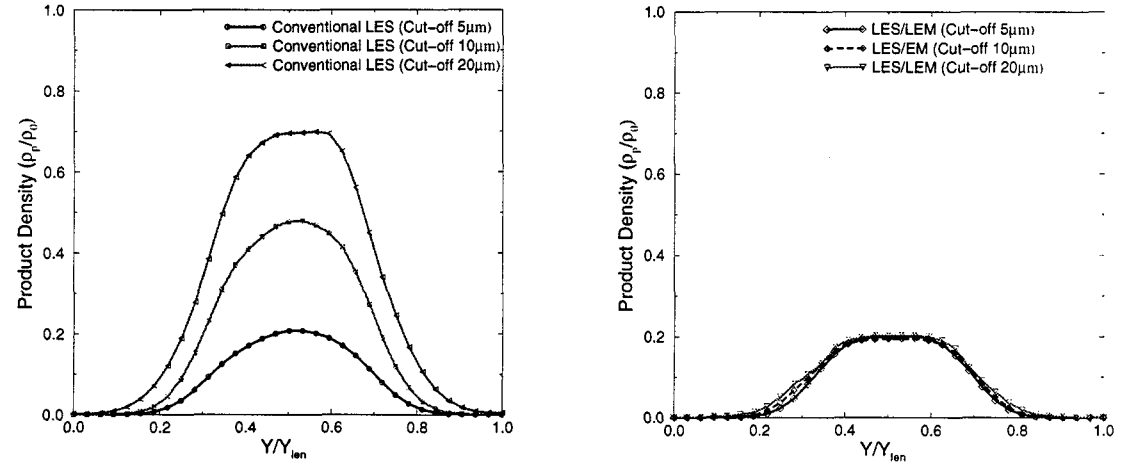

Figure 2: Comparison of the two methods in predicting product density (for infinite rate with Damkohler number Da = ∞) across the mixing layer for different cut-offs. (a) Conventional LES and (b) LEM/LES.

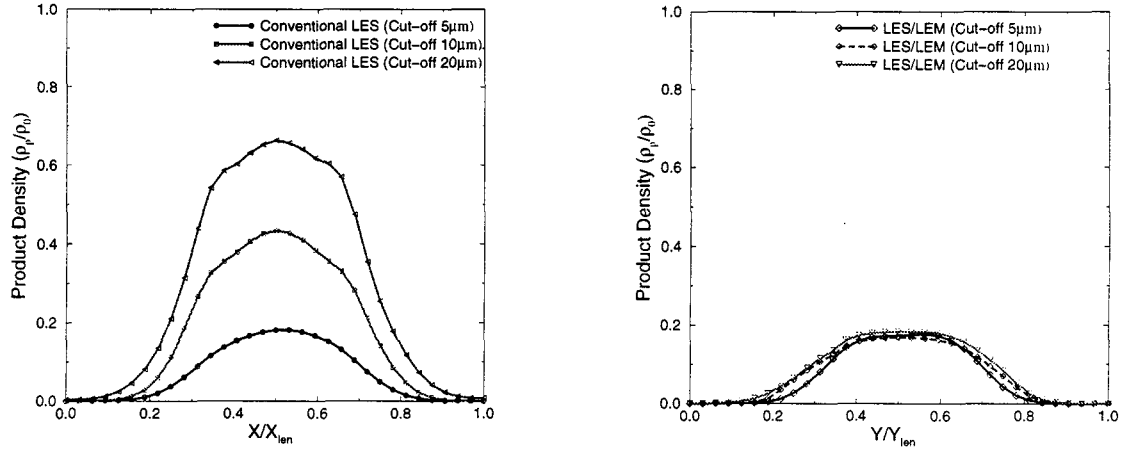

Figure 3: Comparison of the two methods in predicting product density (for finite rate with Damkohler number Da = 100) across the mixing layer for different cut-offs. (a) Conventional LES and (b) LEM/LES.

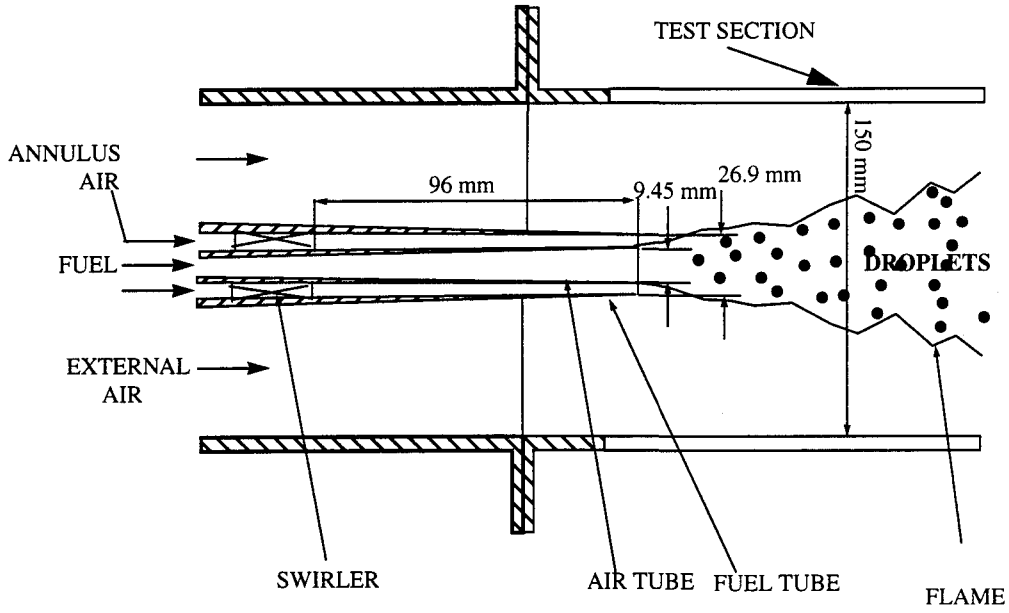

Figure 4: Geometry of the simulated spatial co-axial jet with particle injection.

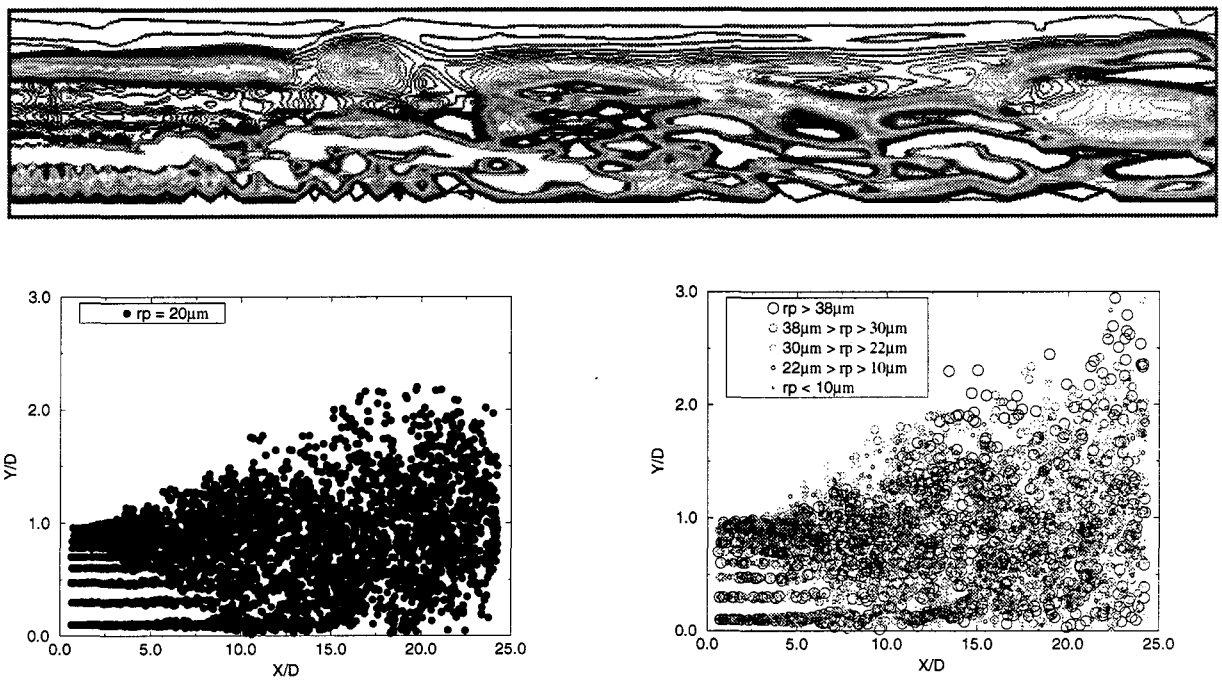

Figure 5: Spatial co-axial jet simulation with droplet injection. (a) Spanwise vorticity contours, (b) Droplet distribution (with single sized particles) and (c) Droplet distribution (with variable sized particles).

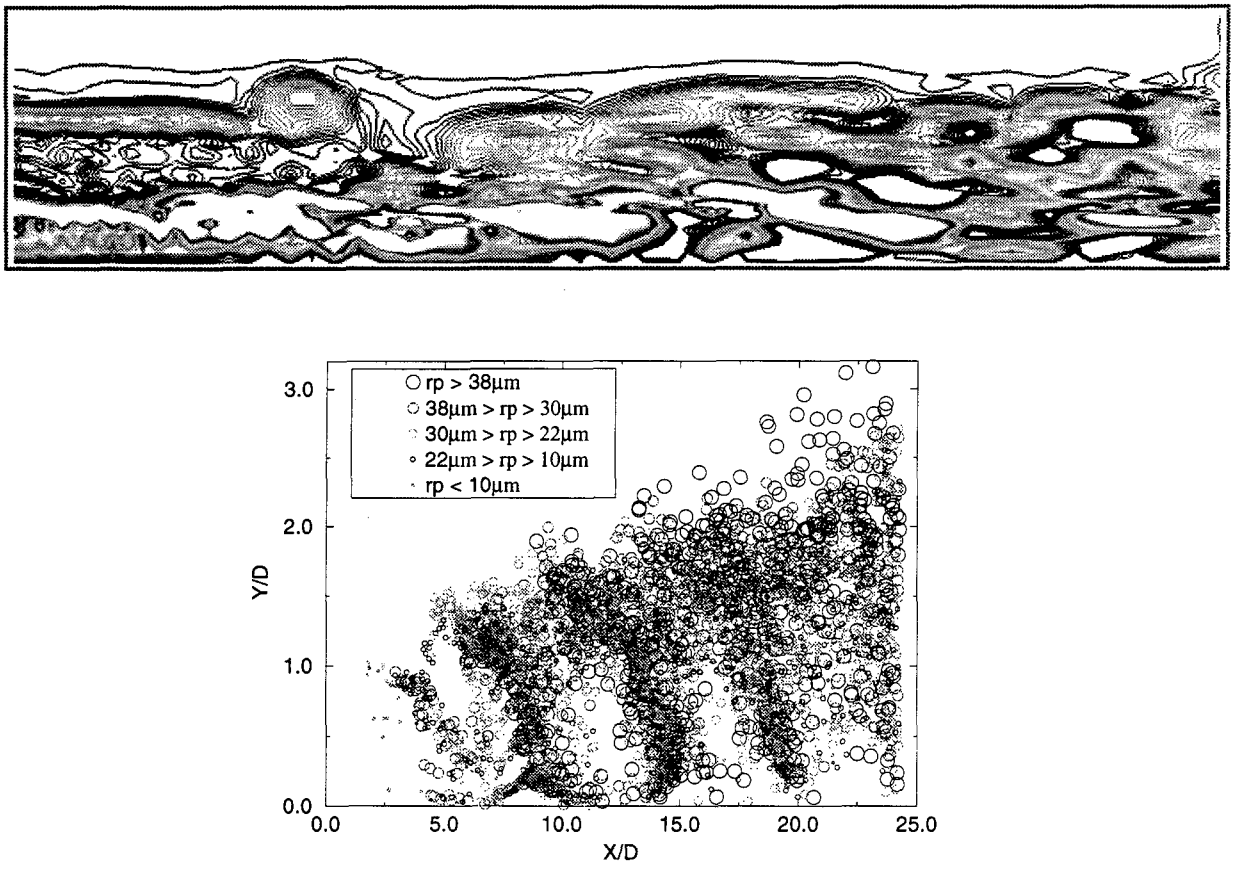

Figure 6: Spatial co-axial jet simulation with variable-size droplet injection and forced inner jet. (a) Spanwise vorticity contours and (b) Droplet distribution.

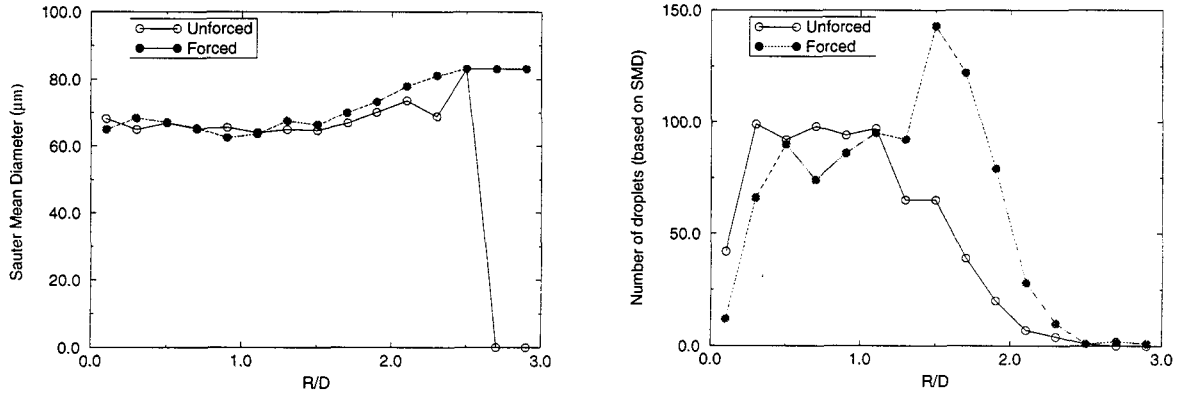

Figure 7: Comparison of the droplet dispersion across the jet for both the forced and unforced cases. a) Radial profiles of SMD at X/D of 17.5 and b) Radial variation of number (computed using SMD) of particles.